A New Half-bridge Resonant Inverter with Load-Freewheeling Modes

Jae-Eul Yeon*, Kyu-Min Cho and Hee-Jun Kim†**

Abstract – This paper presents a new circuit topology and its digital control scheme for a half-bridge resonant inverter. As the proposed half-bridge inverter can be operated in load-freewheeling modes, the pulse-width modulation (PWM) method can be used for the output power control. The proposed half-bridge inverter is based on the resonant frequency-tracking algorithm with the goal of maintaining the unity of the output displacement factor of the load impedance even in varying conditions. In this paper, the operation principle, electrical characteristics, and detailed digital control scheme of the proposed half-bridge resonant inverter are described. The experimental results of the prototype experimental setup to verify the validity of the proposed half-bridge inverter are presented and discussed.

Keywords: High displacement factor control method, Load freewheeling modes, Resonant current tracking algorithm, PWM Half bridge resonant inverter

1. Introduction

High-frequency resonant inverters are widely used in many applications, such as induction heating systems, electronic ballasts, and ultrasonic motor-driving systems [1-7]. Since resonant inverters work at high frequencies, switching losses strongly affect system efficiency. Therefore, zero-voltage switching (ZVS) and zero-current switching (ZCS) techniques are used to reduce the stress of switching devices and to increase system efficiency. Pulse-width modulation (PWM) and pulse-frequency modulation (PFM) methods are also used to control the output power of the resonant inverter [8-10].

The output stage of an inverter consists of loads and resonant factors, L and C, and the resonant frequency varies by the conditions of the resonant factors. Therefore, the most effective strategy to control the output power of the inverter is to make the switching frequency of the inverter track its own resonant frequency.

Pulse-width modulation (PWM) and pulse-frequency modulation (PFM) methods are used to control the output power of the resonant inverter. In the case of the PWM control, the phase-shift switching method is used to decrease the harmonics in the output voltage of the inverter, as well as when a resonant frequency-tracking algorithm is adapted to the phase-shift switching method, the unity of the output displacement factor (DPF) of the output of the inverter can be maintained. However, the PWM control method can be only adapted in a full-bridge inverter, but not in a conventional half-bridge inverter, because the conventional half-bridge inverter cannot operate in load-freewheeling modes. As a half-bridge inverter has several advantages such as having a small number of switching devices and low conduction losses in comparison with a full-bridge inverter, it is widely used in many applications. The PFM control method is the only way to control the output power for the half-bridge resonant inverter. In the PFM control method, the output frequency is set higher than the load resonant frequency to achieve the ZVS. Consequently, the inverter works with lower output power factor when the output power is as low. Sometimes the low power factor operation results in low efficiency, although the switching losses are decreased by the ZCS or the ZVS scheme. This drawback is stronger in a larger-scale system [11, 12].

In response to these concerns, this paper proposes a new circuit topology for the half-bridge resonant inverter, which provides load-freewheeling modes. As the proposed half-bridge inverter can be operated in load-freewheeling modes, the PWM control method can be used for the output power control. Also, a novel PWM scheme based on the load-resonant frequency-tracking algorithm is also proposed.

In this paper, the fundamental principles and electrical characteristics, and detailed digital control scheme of the proposed half-bridge inverter and PWM control method are described. The experimental results using a prototype experimental setup for the RLC series resonant load are presented and discussed.

† Corresponding Author: School of Electrical Engineering and Computer Science, Hanyang University, Korea. (hjkim@hanyang.ac.kr)
* Visual System Team/HVFPG, Fairchild Semiconductors, Korea. (jeyeon@fairchildsemi.co.kr)
** Dept. of Information and Communications, Yuhan Collage, Korea. (limsa@yuhan.ac.kr)
Received 10 August, 2006 ; Accepted 16 January, 2007

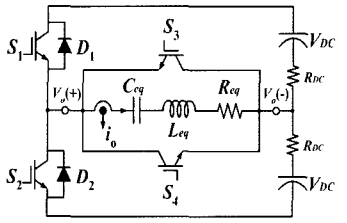

Fig. 1. Configuration of the proposed half-bridge resonant inverter.

2. Half-Bridge Resonant Inverter with Load-Freewheeling Modes

2.1 Configurations of the Main Circuit

Fig. 1 shows the circuit configurations of the proposed half-bridge inverter. Two switching devices, *S3* and *S4*, are added to the conventional half-bridge inverter, which provide the load-freewheeling modes. Switching devices without non-inverse parallel diodes must be used for *S3* and *S4*, and these can be replaced by thyristors. Conventional switching devices can be used for *S1* and *S2*, although the freewheeling diodes, *D1* and *D2*, should not be conducted in any operational modes. The output voltage and current waveforms, switching patterns and the conduction durations of the switching devices are shown in Fig. 2, and the current paths for each mode are shown in Fig. 3.

The proposed half-bridge inverter uses a novel PWM method that employs the resonant frequency-tracking algorithm to control the output power of the inverter. When the main switches, *S*1 and *S*2, in Fig. 1 are on-state, the powering modes are provided in a way similar to that of the conventional half-bridge inverter. However, during the off-state of main switches, the auxiliary switches *S*3 and *S*4 are conducted. Consequently, the load-freewheeling modes are provided and the output voltage of the inverter becomes zero. As a result, the output voltage of the inverter is generated at the center of the resonant current, therefore the output DPF can always be kept in unity allowing the inverter to work more efficiently.

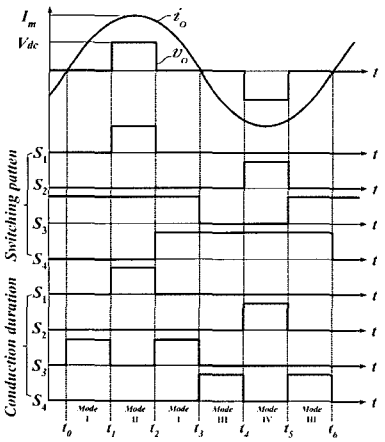

Fig. 2. Output voltage and current, switching patterns, and conduction durations.

2.2 Detailed Switching Scheme

In the positive-current mode, the on time, *Tons1*, and off time, *Toffs1*, of the switch *S1* are calculated as follows:

$$T_{ons1} = (T_s - T_d)/2 \tag{1}$$

and

$$T_{offs1} = (T_s + T_d)/2 \tag{2}$$

respectively.

While the resonant current is positive, the switch, *S*3 maintains an on-state. On the other hand, while the resonant current is negative, the switch, *S*4 maintains an on-state. Consequently, the load-freewheeling modes are achieved.

Figs. 4 and 5 show an example of the controller to generate the proposed switching signal and its specific timing diagram. The presented controller is designed as a fully digital circuit. It can also be designed with a microprocessor; however, a discrete digital circuit using an erasable programmable logic device (EPLD) is more reliable and economical for high-frequency applications. The digital circuit can be constructed using approximately 5000-gates EPLD, in case of an 8-bit resolution system.

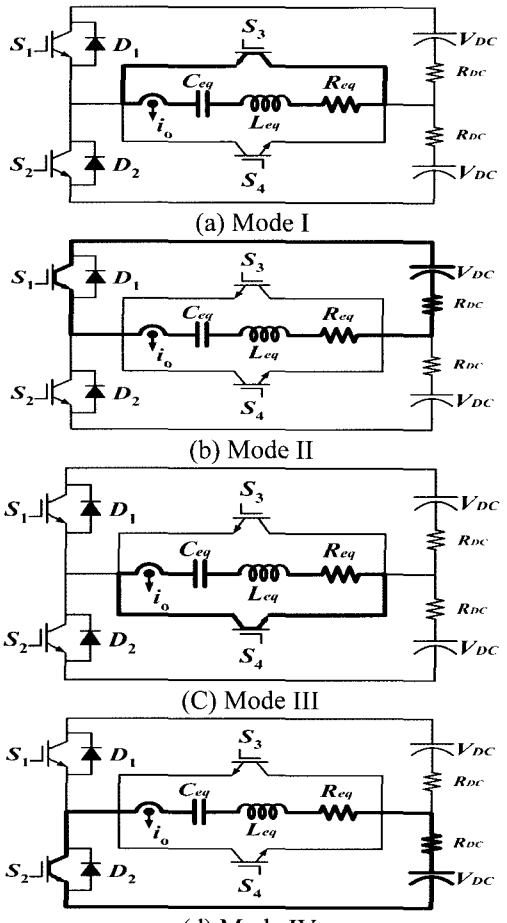

Fig. 3. Current paths for each mode.

2.3 Output Characteristics of the Conventional Half-bridge Inverter

The switching frequency of the conventional half-bridge inverter is always higher than the resonant frequency to achieve ZVS or ZCS. Also, because only the PFM method is applied to control the output power of the inverter, the lower the output power of the inverter, the worse its total efficiency. The *rms* fundamental output voltage of the conventional half-bridge inverter is given by The output power and power factor (*PF*) of the conventional half-bridge inverter is given by equations (4) and (5), respectively.

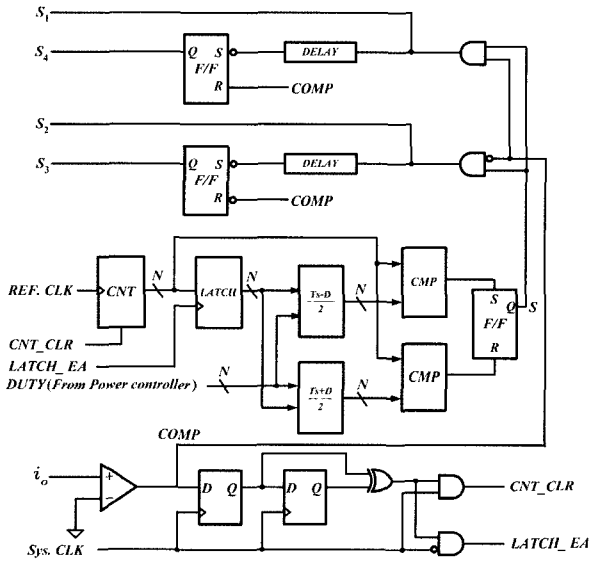

Fig. 4. Fully digital switching signal generator.

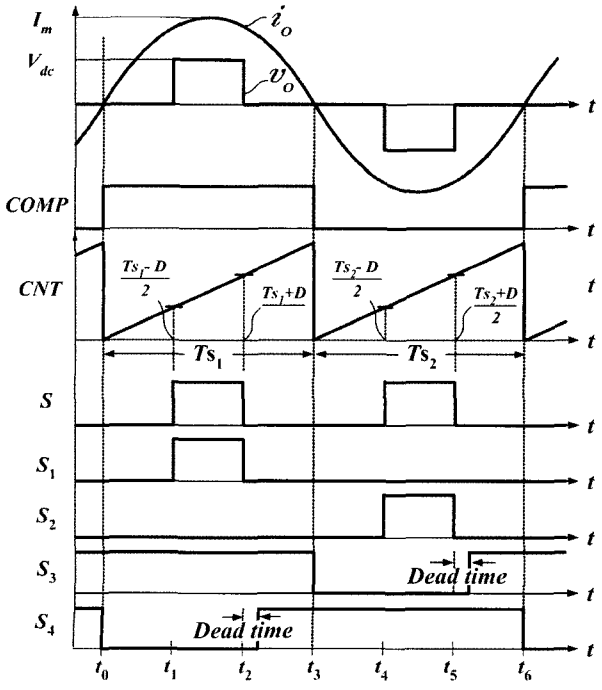

Fig. 5. Specific timing diagram.

$$V_{O1(1)} = \frac{2\sqrt{2}}{\pi} V_{DC} \tag{3}$$

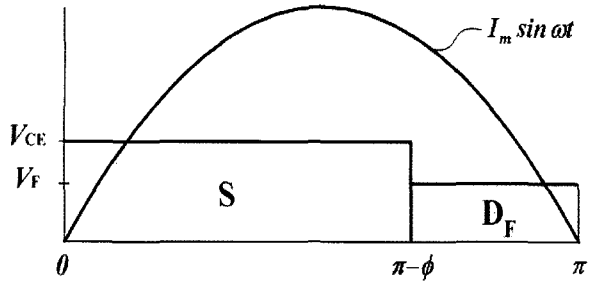

Fig. 6. Conduction period for half cycle of the conventional inverter.

$$P_{O(1)} = \frac{2\sqrt{2}}{\pi} V_{DC} I_{O(1)} \cos\phi \tag{4}$$

$$PF_{(1)} = \frac{2\sqrt{2}}{\pi} \cos\phi \tag{5}$$

2.4 Switch Loss Analysis of the Conventional Half-bridge Inverter

When the switching duty ratio is 100% and there is no phase difference between the output voltage and resonant current, the output power of the conventional half-bridge inverter becomes the maximum value.

Assuming that the resonant current *io* is purely sinusoidal, the total losses of switches by the variation of the output power can be calculated. Fig. 6 shows the conduction period for the half cycle of the conventional half-bridge inverter.

Because the switching devices of the conventional half-bridge inverter are turned on or turned off under ZVS or ZCS, only conduction loss, *P*lc(1) is sustained. Therefore, total switch loss, *Pts*(1) is given by the equation:

$$P_{ts(1)} = P_{lc(1)} = \frac{I_m}{\pi}\left[V_{CE\_sat}\{1-\cos(\pi-\phi)\} + V_F\{1+\cos(\pi-\phi)\}\right] \tag{6}$$

2.5 Output Characteristics of the Proposed Half-bridge Inverter

When the switching duty ratio is 100% and there is no phase difference between the output voltage and resonant current, the output power of the conventional half-bridge inverter becomes the maximum value. Assuming that the resonant current *io* is purely sinusoidal, the total losses of s The duty ratio *D* of the proposed method is defined as follows:

$$D = \frac{T_d}{T_s} \tag{7}$$

where *Td* is conduction duration and *Ts* is switching period.

According to the proposed method, the *rms* value, *Vo* and the fundamental component, *Vo*1(2) of the output voltage of the inverter are given by equations (8) and (9), respectively:

$$V_o = V_{dc}\sqrt{D} \tag{8}$$

$$V_{o1(2)} = \frac{2\sqrt{2}}{\pi} V_{dc} \sin\frac{D}{2}\pi \tag{9}$$

Assuming that the resonant current *io* is sinusoidal, the *rms* value of the output current, *Io*(2) is derived as

$$I_{o(2)} = \frac{2\sqrt{2}}{\pi R_{eq}} V_{dc} \sin\frac{D}{2}\pi \tag{10}$$

where *Req* is the equivalent resistance of the load. Therefore, the output power *Po*(2) is given by

$$P_{o(2)} = \frac{8}{\pi^2 R_{eq}} V_{dc}^{\ 2} \sin^2\frac{D}{2}\pi \tag{11}$$

Although the output displacement factor is controlled in unity under the proposed method, the output power factor is not unified because output voltage is inevitably rectangular. The output power factor and the total harmonic distortion (*THD*(2)) of the output voltage according to the duty ratio *D* is respectively expressed by:

$$PF_{(2)} = \frac{2\sqrt{2}}{\sqrt{D}\pi} \sin\frac{D}{2}\pi \tag{12}$$

and

$$THD_{(2)} = \sqrt{\frac{D\pi^2}{4(1-\cos D\pi)} - 1} \tag{13}$$

Fig. 7 shows the comparison results of the output characteristics between the proposed half-bridge inverter and the conventional half-bridge converter where the number "1" refers to the conventional method and the number "2" refers to the proposed method. The output power, power factor, and *THD* of the output voltage are plotted according to the duty ratio *D*. When the duty ratio is greater than 0.5, the output power factor of the proposed half-bridge inverter is always greater than 0.9 while that of the conventional type has a poor power factor in the whole output range. Also, the *THD* of the proposed half-bridge inverter is also lower than the conventional type when the duty ratio is greater than 0.5. From the above results, when the inverter output exceeds half of the maximum output capacity, the output power factor is relatively high. This is the reason that the displacement factor of the proposed method is uniformly maintained.

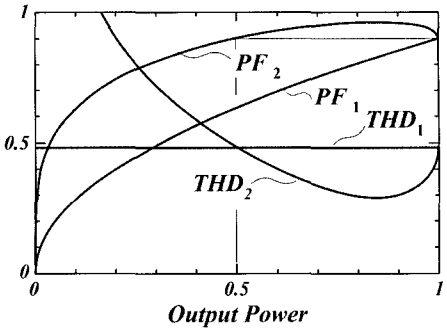

Fig. 7. Comparison of output characteristic of the proposed inverter with the conventional type

If the resonance *Q*-factor is not high, many harmonics are injected in the output voltage, resulting in a distorted current waveform output. Therefore, it is recommended that the inverter should be operated in the low *THD* region—the high power factor region—when the resonance *Q*-factor is not high.

2.6 Losses Analysis of the Proposed Half-bridge Inverter

Since the proposed half-bridge inverter turns on and off under the hard switching condition, whereas the conventional type operates under the zero voltage condition, it cannot avoid switching losses. The conduction and switching periods of the proposed half-bridge inverter are shown in Figs. 8 and 9, respectively.

As the on-state voltage drop of the switching device is *VCE*, forward voltage drop of the diode is *VF*, turn-on time and turn-off time are δ_1 and δ_2, respectively, then the theoretical conduction losses and switching losses of the switching devices, *Plc* and *Pls*(2), is calculated by

$$P_{cl} = \frac{2V_{CE} I_m}{\pi} \tag{14}$$

and

$$P_{ls(2)} = \frac{\omega V_{DC}}{6\pi}\left[\left\{\delta_1 I_m \sin\omega\left(\frac{(1-D)\pi}{2\omega}+\delta_1\right)+I_m \sin\omega\left(\frac{(1-D)\pi}{2\omega}\right)\right\} + \delta_2\left\{I_m \sin\omega\left(\frac{(1+D)\pi}{2\omega}\right)+I_m \sin\omega\left(\frac{(1+D)\pi}{2\omega}+\delta_2\right)\right\}\right] \tag{15}$$

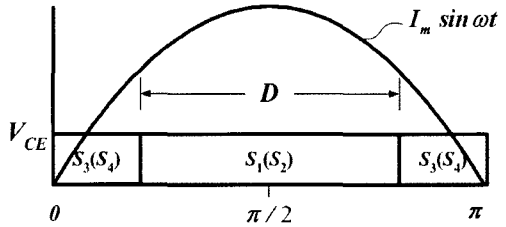

Fig. 8. Conduction period of the proposed inverter

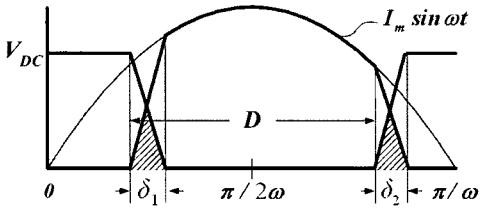

(a) $S1$, $S2$

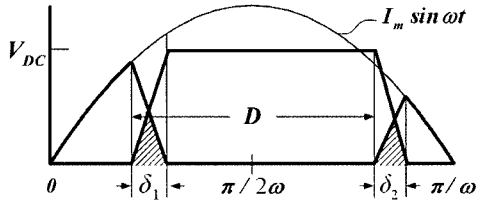

(b) $S3$, $S4$

Fig. 9. Switch voltage and current of the proposed inverter

Therefore, total switching losses are calculated as follows:

$$P_{ts(2)} = \frac{2V_{CE}I_m}{\pi} + \frac{\omega V_{DC}}{6\pi}\left[\left\{\delta_1 I_m \sin\omega\left(\frac{(1-D)\pi}{2\omega}+\delta_1\right)\right.\right.$$
$$+I_m \sin\omega\left(\frac{(1-D)\pi}{2\omega}\right)\Big\}+\delta_2\left\{I_m \sin\omega\left(\frac{(1+D)\pi}{2\omega}\right)\right.$$
$$\left.\left.+I_m \sin\omega\left(\frac{(1+D)\pi}{2\omega}+\delta_2\right)\right\}\right] \quad (16)$$

3. Simulation and Experimental Results

3.1 System Efficiency Characteristics

The principal parameters of the simulation are shown in Table 1. From the parameters in Table 1, the resonant frequency, *fo* and the maximum output power, *P*omax are determined as 30.08 kHz and 5 kVA. The maximum value of the resonant current of the conventional half-bridge inverter, *I*m(1) is calculated as follows:

$$I_{m(1)} = \frac{\sqrt{2}V_{o1}}{Z} = \frac{4V_{DC}}{\pi Z} \quad (17)$$

Table 1. Parameters of the simulation

Parameter	Value
VDC	100 V
δ_1	30 *nsec*
δ_2	100 *nsec*
Req	2 Ω
ESRDC	200 *m*Ω
L	200 *u*H
C	140 *n*F
VCE	1.8 V
VF	1.2 V

where,

$$Z = \sqrt{R^2 + \left(\omega L - \frac{1}{\omega C}\right)^2} \quad (18)$$

On the other hand, the maximum value of the resonant current of the proposed type, *I*m2 is calculated as follows:

$$I_{m(2)} = \sqrt{2}I_o = \frac{4}{\pi R_{eq}} V_{DC} \sin\left(\frac{D\pi}{2}\right) \quad (19)$$

The output efficiencies of the conventional ($\eta o(1)$) and the proposed ($\eta o(2)$) half-bridge inverter are defined in the following equations:

$$\eta_{o(1)} = \frac{P_{o1}}{P_{o1} + P_{ts1}} \quad (20)$$

$$\eta_{o(2)} = \frac{P_{o2}}{P_{o2} + P_{ts2}} \quad (21)$$

The calculated output efficiencies from equations (20) and (21) are plotted in Fig. 10, which shows that the efficiency of the conventional half-bridge inverter is higher than the proposed type in the whole output range because switching devices are turned on and off under zero voltage condition, whereas the proposed type operates with hard switching.

The input current of the conventional half-bridge inverter flows during the whole period. But with the proposed type, the input current only flows while the main switches, *S*1 or *S*2 are conducted. Therefore, the average input current of the conventional (*Ii*(1)) and the proposed (*Ii*(2)) half-bridge inverter are defined as follows:

$$I_{i(1)} = \frac{2I_{m1}}{\pi} \quad (22)$$

and

$$I_{i(2)} = \frac{I_{m1}}{\pi}\left\{\cos\left(\frac{\pi - D\pi}{2}\right) - \cos\left(\frac{\pi + D\pi}{2}\right)\right\} \quad (23)$$

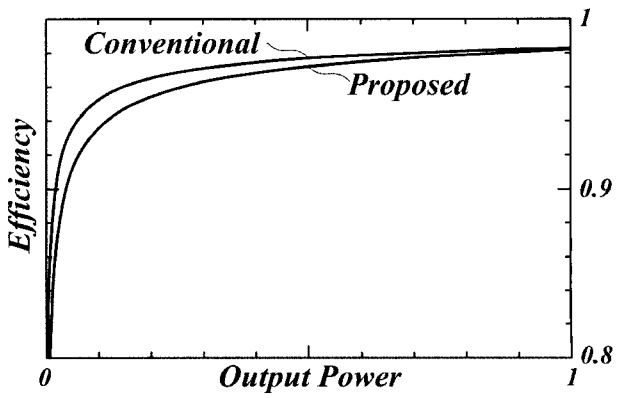

Fig. 10. Output efficiency comparison

From equations (22) and (23), the losses occurring at *RDC*, the equivalent series resistance of the DC link voltage, *Pi*(1) and *Pi*(2) are

$$P_{i(1)} = \frac{4I_{m(1)}{}^2 R_{DC}}{\pi^2} \quad (24)$$

$$P_{i(1)} = 4R_{DC}\sin^2\frac{D\pi}{2} \quad (25)$$

The input efficiencies of the conventional ($\eta i(1)$) and the proposed ($\eta i(2)$) half-bridge inverter are

$$\eta_{i(1)} = \frac{P_{o1}}{P_{o1} + P_{i1}} \quad (26)$$

$$\eta_{i(2)} = \frac{P_{o2}}{P_{o2} + P_{i2}} \quad (27)$$

Therefore, the total efficiencies of the conventional ($\eta t(1)$) and the proposed ($\eta t(2)$) half-bridge inverter are defined in the following equations:

$$\eta_{t(1)} = \frac{P_{o(1)}}{P_{o(1)} + P_{ts(1)} + P_{i(1)}} \quad (28)$$

$$\eta_{t(2)} = \frac{P_{o(2)}}{P_{o(2)} + P_{ts(2)} + P_{i(2)}} \quad (29)$$

The calculated input efficiencies from equations (26) and (27) are plotted in Fig. 11, and the calculated total efficiencies from equations (28) and (28) are plotted in Fig. 12. The efficiency of the proposed half-bridge inverter is higher than the conventional type in the whole output range, especially when the inverter works with a light load. In such a case, the total efficiency of the proposed half-bridge inverter is relatively high.

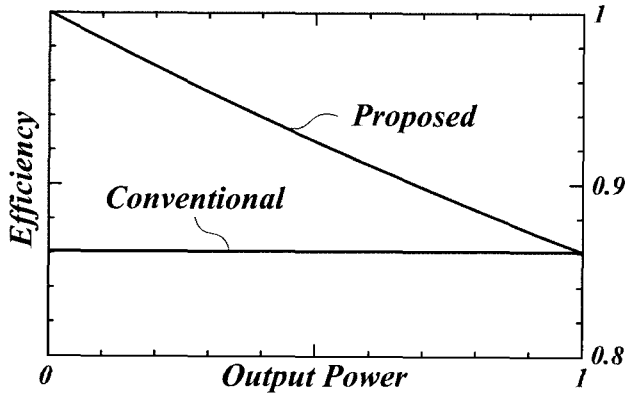

Fig. 11. DC link efficiency comparison

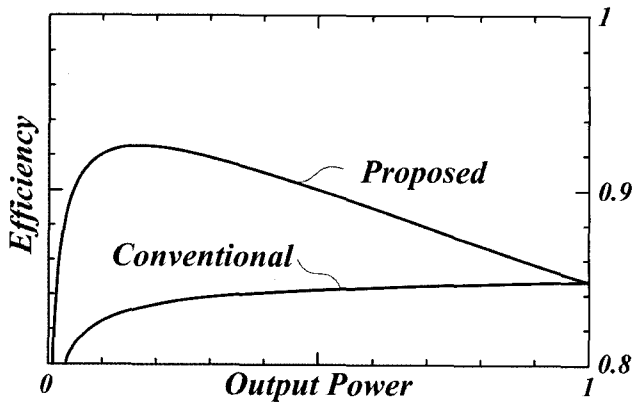

Fig. 12. Total system efficiency comparison

3.2 Experimental Results

A prototype inverter was built and tested, and the experimental parameters are as follows:

- DC link voltage: 110 *VDC*
- Equivalent inductance: 240 *uH*
- Equivalent capacitance: 100 *nF*
- Equivalent resistance: 10 Ω

In this case, the series resonant frequency is about 35.6 kHz. Fig. 13 shows the experimental power losses measured on the switching devices and the system efficiency of the proposed half-bridge inverter. The proposed inverter has better efficiency than that of the conventional half-bridge inverter in the whole output power range, where the maximum output power is about 64 W. In the full power range, however, the conventional half-bridge inverter has the same output power factor compared to the proposed inverter. Fig. 14 presents the output voltage and current waveforms at 20% duty and 80% duty. It can be seen that the output displacement factor is uniformly maintained and the proposed PWM method is well adopted.

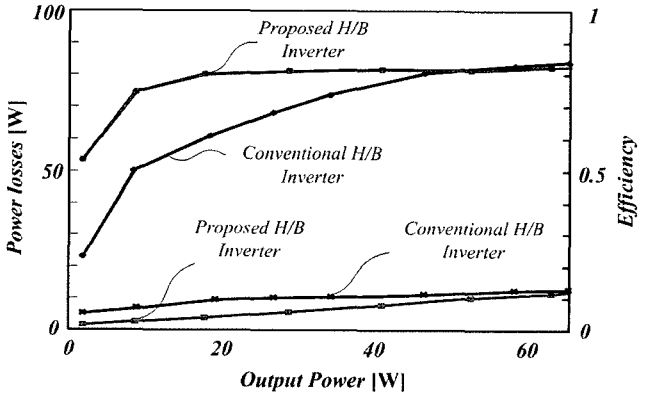

Fig. 13. Experimental measured power losses and efficiency

4. Conclusion

This paper proposed a new circuit topology of the half-bridge resonant inverter with load-freewheeling

modes and its digital control scheme. As the proposed half-bridge inverter can operate with load-freewheeling modes, the pulse-width modulation (PWM) method can be adopted to control the power output. Therefore, even if the load impedance varies, the output displacement factor (DPF) can be maintained in unity. In this paper, the electrical characteristics and switching losses of the proposed inverter are analyzed and compared with a conventional half-bridge resonant inverter. As a result, the total system efficiency of the proposed inverter is determined to be superior to that of the conventional inverter in most power ranges. With the experimental results of the prototype experimental setup, the validity of the proposed half-bridge resonant inverter is verified.

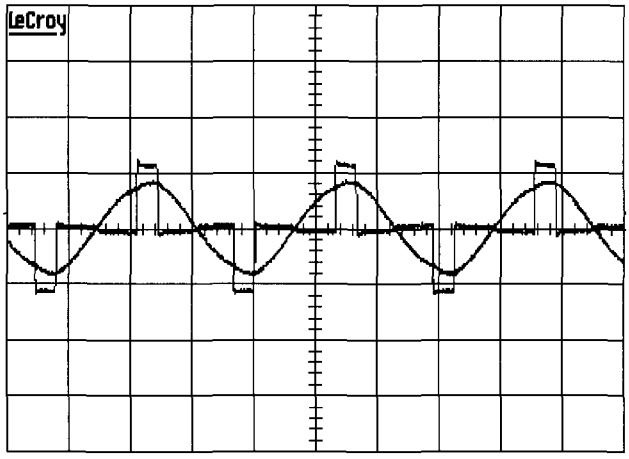

(a) at 20% duty

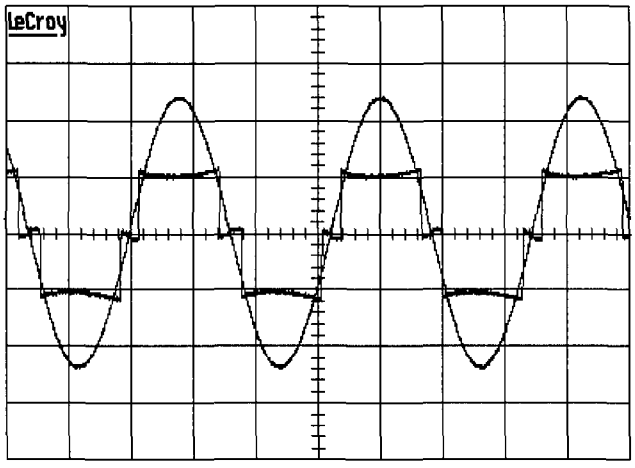

(b) at 80% duty

Fig. 14. Output voltage and current waveforms of the proposed half-bridge inverter

References

[1] Alonso, J.M.; Rico, M.; Blanco, C.; Lopez, E., "A Novel Low-Loss Clamped-Mode LCC Resonant Inverter for HID Lamp Supply", IEEE-PESC Conf. Rec., pp. 736-742, 1995.

[2] Grajales, L.; Sabate, J.A.; Wang, K.R.; Tabisz, W.A.; Lee, F.C. ,"Design of a 10kW, 500 kHz Phase-Shifted Controlled Series-Resonant Inverter for Induction Heating", IEEE-IAS Conf. Rec., Vol. 2, pp. 843-849, 1993.

[3] Izaki, K.; Hirota, I.; Yamashita, H.; Omori, H.; Wang, S.P.; Jasni, Md.; Nakaoka, M., "Soft-Switched PWM High-Frequency Load-Resonant Inverter with Power Factor Correction for Induction Heating Cooking Appliance", EPE Conf. Rec., Vol. 2, pp. 244-249, 1997.

[4] Furuya, S.-i.; Maruhashi, T.; Izuno, Y.; Nakaoka, M., "Load-Adaptive Frequency Tracking Control Implementation of Two-Phase Resonant Inverter for Ultrasonic Motor", IEEE Trans. on PE, Vol. 7, No. 3, pp. 542-550, July 1992.

[5] Okudaira, S.; Nomura, K.; Matsuse, K., "New quasi-resonant inverter for induction heating", Power Conversion Conf. Rec., pp. 117-122, 1993.

[6] Mertens, A.; Skudelny, H.-C., "Switching losses in a GTO inverter for induction heating", IEEE Transactions on PE, Vol. 6 Issue 1, pp. 93-99, 1991.

[7] Ogiwara, H.; Okuno, A.; Nakaoka, M., "High frequency induction heating load resonant inverter with voltage-clamped quasi-resonant switched using newly-improved static induction transistors/thyristors and their phase shifted controlled scheme", IAS Conf. Rec. Vol. 1, pp. 941-948, 1992.

[8] Ammar, A.; El-Bakry, M.; Godah, H.M., "Application of pulse frequency modulation for voltage frequency control of inverters", SICE Conf. pp. 1565 – 1570, 1995.

[9] Liu, Y.; He, X.; "PDM and PFM hybrid control of a series-resonant inverter for corona surface treatment", Electric Power Applications, IEE Proceedings - Vol. 152, pp. 1445 - 1450 Nov. 2005

[10] G. C. Hsieh and C. M. Wang, "One-cycle controlled half-bridge series-resonant DC to AC inverter with reduced conduction loss", IEEE-IECON Conf., pp. 786–791. 1997

[11] Jae-Eul Yeon; Kyu-Min Cho; Won-Seok Oh; Hee-Jun Kim, "A novel half-bridge resonant inverter having load-freewheeling modes", IEEE-PESC Conf., pp. 1304 – 1307, Vol. 2, May 2004.

[12] Kyu-Min Cho; Won-Seok Oh; Jae-Eul Yeon; Hee-Jun Kim, "A new switching scheme for resonant inverters using a resonant-frequency tracking algorithm", IEEE-IECON Conf., pp. 2580 - 2585 Vol. 3, Nov. 2003.

Jae-Eul Yeon
received his B.S. and M.S. degrees in Electrical Engineering from Hoseo University, Asan, Korea, in 2000 and 2002, respectively and his Ph.D. degree in Mechatronics Engineering from Hanyang University, Ansan, Korea. He is currently working for Fairchild Semiconductor. His research interests are in functional power module, flat panel displays, resonant inverters, soft switching dc/dc converters, and electronic ballast. He is currently a member of the Korean Institute of Electrical Engineers, and the Korean Institute of Power Electronics.

Kyu-Min Cho
received his B.S., M.S., and Ph.D. degrees in Electrical Engineering from Inha University, Incheon, Korea, in 1985, 1991, and 1994, respectively. Since 1995, he has been with Yuhan College, Pucheon, Korea, where he is currently a Professor of the Department of Information and Communications. His research interests include communications power supply, electronic ballasts, switching techniques of power converters, and high-frequency power sources for plasma applications. Dr. Cho is a member of the Korean Institute of Electrical Engineers, the Institute of Electronics Engineers of Korea, and the Korean Institute of Power Electronics.

Hee-Jun Kim
received his B.S. and M.S. degrees in Electronics Engineering from Hanyang University, Seoul, Korea, in 1976 and 1978, respectively, and his Ph.D. degree in Electronics Engineering from Kyushu University, Kyushu, Japan, in 1986. Since 1987, he has been with the School of Electrical Engineering and Computer Science, Hanyang University, Ansan, Korea, where he is currently a Professor. From 1991 to 1992, he was with the Virginia Polytechnic Institute and State University, Blacksburg, as a Visiting Scholar. His fields of interest include switching power converters, electronic ballast, soft switching techniques, and analog signal processing. Dr. Kim is a Fellow of the Korean Institute of Electrical Engineers, the Institute of Electronics Engineers of Korea, and the Korean Institute of Power Electronics.